# Constrained tricritical phenomena in two dimensions

Youjin Deng,[1,2] Jouke R. Heringa,[2] and Henk W. J. Blöte[2,3]
[1]*Laboratory for Material Science, Delft University of Technology, Rotterdamseweg 137, 2628AL Delft, The Netherlands*
[2]*Faculty of Applied Sciences, Delft University of Technology, P.O. Box 5046, 2600 GA Delft, The Netherlands*
[3]*Lorentz Institute, Leiden University, P.O. Box 9506, 2300 RA Leiden, The Netherlands*
(Received 24 October 2004; published 15 March 2005)

We investigate several tricritical models on the square lattice by means of Monte Carlo simulations. These include the Blume-Capel model, Baxter's hard-square model, and the $q=1$, 3, and 4 Potts models with vacancies. We use a combination of the Wolff and geometric cluster methods, which conserves the total number of vacancies or lattice-gas particles and suppresses critical slowing down. Several quantities are sampled, such as the specific heat $C$ and the structure factor $C_s$, which accounts for the large-scale spatial inhomogeneity of the energy fluctuations. We find that the constraint strongly modifies some of the critical singularities. For instance, the specific heat $C$ reaches a finite value at tricriticality, while $C_s$ remains divergent as in the unconstrained system. We are able to explain these observed constrained phenomena on the basis of the Fisher renormalization mechanism generalized to include a subleading relevant thermal scaling field. In this context, we find that, under the constraint, the leading thermal exponent $y_{t1}$ is renormalized to $2-y_{t1}$, while the subleading exponent $y_{t2}$ remains unchanged.

DOI: 10.1103/PhysRevE.71.036115 PACS number(s): 05.50.+q, 64.60.Cn, 64.60.Fr, 75.10.Hk

## I. INTRODUCTION

In experiments, many systems undergoing phase transitions are subject to external constraints such as the conversation of particle numbers in a mixture. Such systems are described in terms of the canonical ensemble and thus typically display a behavior different from that of unconstrained models, which are described by the grand ensemble. An example is the superfluid transition in the $^3$He-$^4$He mixtures [1], whose universal properties can be described by a dilute $XY$ model. The Hamiltonian of the lattice $XY$ model reads

$$\mathcal{H}/k_{\mathrm{B}}T = -K\sum_{\langle i,j\rangle} \vec{s}_i \cdot \vec{s}_j + D\sum_k |\vec{s}_k|^2, \qquad (1)$$

where the spins can assume a unit vector of two components, $|\vec{s}_k|=1$, or a vacancy $|\vec{s}|=\vec{0}$. The sum $\langle\rangle$ is over nearest-neighbor lattice pairs, and $K$ and $D$ are the coupling constant and the chemical potential of vacancies, respectively. The mole fraction of $^3$He in the experiment corresponds to the vacancy density $\rho=(1/N)\Sigma_k(1-|\vec{s}_k|^2)$, with $N$ the total number of lattice sites. For $D\to-\infty$, the vacancies are excluded, and the model (1) reduces to the pure $XY$ model. In three dimensions, this model undergoes a second-order phase transition, and the critical coupling constant $K_c(D)$ is an increasing function of $D$. The critical line terminates at a tricritical point $(K_t,D_t)$. Since the upper tricritical dimensionality of the $O(n)$ model ($n\geqslant 1$) is equal to 3, significant exact information is available [1]. A set of universal parameters can be exactly obtained by means of mean-field analyses and also by renormalization group (RG) calculations of the Landau-Ginzburg-Wilson Hamiltonian. The leading and subleading thermal critical exponents are $y_{t1}=2$ and $y_{t2}=1$ [1]. Thus, as the tricritical point is approached, one simply expects that the specific heat $C$ diverges with index $\alpha=2-3/y_{t1}=1/2$. We mention that, as generally expected, the tricritical scaling behavior at three dimensions suffers from logarithmic corrections whose expressions can be found in Ref. [1]. However, typical experiments take place at a constant density $\rho$ instead at a constant chemical potential $D$. It was reported [2] that, at the tricritical point $(K_t,\rho_t)$, the specific heat $C$ has only a finite value with $\alpha=-0.9(1)$, apparently different from the aforementioned index $\alpha=1/2$. Thus, the theoretical description of the experiment in Ref. [2] uses the dilute $XY$ model with a *conserved* number of vacancies. This means that an external constraint is imposed on the system (1). Since the pertinent $^3$He and $^4$He mixtures are liquid, the constraint is of the "annealed" type [3]. Therefore, the vacancies should be able to move freely over the lattice of model (1).

The effect of a constraint on a critical systems has already been studied for decades [3–6]. As early as in 1965, Syozi introduced [4] a decorated Ising model, which is intimately connected with annealed systems. The Syozi model can be exactly transformed into the spin-$\frac{1}{2}$ model, and for dimensionality $d>2$ the critical exponents of these two models are related as

$$\alpha_{\mathrm{s}} = -\alpha/(1-\alpha), \quad \beta_{\mathrm{s}} = \beta/(1-\alpha), \quad \nu_{\mathrm{s}} = \nu/(1-\alpha), \quad \ldots, \qquad (2)$$

where $\alpha$ and $\beta$ are the standard critical indices for the specific heat $C$ and the magnetization density $m$, respectively, and $\nu=1/y_t$ is the inversion of the thermal exponent. The subscript "s" represents the Syozi model. Later, this constraint mechanism was discussed in a more general context by Essam and Garelick [5] and by Fisher [6]. It was argued [5,6] that the relations (2) are not specific to the Syozi model, but are more generally satisfied by equilibrium models with a divergent specific heat $C$. Thus, Eq. (2) predicts that, as long as $\alpha>0$, the constrained critical specific heat $C$ can at most reach a *finite* value instead of being divergent. For systems with a convergent specific heat $\alpha<0$, Fisher [6] pointed out that no renormalization of critical exponents as Eq. (2) oc-

 

curs, but additional corrections can be introduced by the constraint. Further, for the marginal case $\alpha=0$—i.e., $C$ normally diverges logarithmically in unconstrained systems—it was shown [6] that, again, the constraint leads to a convergent specific heat. Since then, Fisher's *renormalized* critical exponents have been used extensively [3,7–10].

More general theories were then formulated for constrained systems, including a theory of constrained tricritical phenomena [11,12]. Besides vacancies, constraints can be imposed on volumes or pressure, etc. It was argued [11,12] that, depending on the type or strength of the constraint, a continuous transition may become Fisher renormalized, remain unchanged, or become first order. The special point where the transition remains unchanged was referred to as a special "tricritical" point [11].

In the context of the RG theory, Imry and co-workers [13] applied the $\epsilon$-expansion technique to a generalized Landau-Ginzburg-Wilson Hamiltonian. The effect of the constraint is accounted for by an additional parameter, and they found four distinct fixed points: the tricritical Ising (TI), the critical Ising (CI), the *renormalized* tricritical Ising (RTI), and the *renormalized* critical Ising (RCI) fixed point. The critical exponents at these fixed points are related as $\alpha_{\mathrm{RCI}}=-\alpha_{\mathrm{CI}}/(1-\alpha_{\mathrm{CI}})$ and $\alpha_{\mathrm{RTI}}=-\alpha_{\mathrm{TI}}/(1-\alpha_{\mathrm{TI}})$, in agreement with Eq. (2). For the spatial dimensionality $d\geqslant 3$, TI and RTI correspond to Gaussian and spherical fixed points, respectively [13]. Thus, at the fixed points TI and RTI, the critical index is equal to $\alpha_{\mathrm{TI}}=1/2$ and $\alpha_{\mathrm{RTI}}=-1$, respectively. For the $^3$He—$^4$He mixtures, if one assumes that constrained tricritical behavior is governed by the fixed point RTI, the theoretical prediction $\alpha_{\mathrm{RTI}}=-1$ is in good agreement with the experimental result $\alpha=-0.9(1)$ [2].

However, to our knowledge, numerical tests of these theories are still scarce; in particular, the finite-size behavior of constrained critical systems has only attracted limited attention. Thus, very recently, we performed [14] a Monte Carlo investigation of the constrained three-dimensional Blume-Capel (BC) model [15,16]. The phase diagram of the BC model is analogous to that of the dilute $XY$ model, and in three dimensions, the two tricritical models share a common set of critical exponents. At the tricritical point, the constrained specific heat reaches a finite value with the index $\alpha=-0.99(3)$ [14], in agreement with the experimental data [2] and the RG calculations in Ref. [13]. Nevertheless, the exponent of the power law describing the decay of the correlation function at tricriticality remains unchanged under the constraint. In this sense, the constraint does not lead to a change of the universality class. In Ref. [14], we also generalized Fisher's approach [6] for application to *tricritical* systems. For the tricritical BC model in three dimensions, this mechanism also predicts that the unconstrained and constrained indices are related as $\alpha^{\mathrm{co}}=-\alpha^{\mathrm{un}}/(1-\alpha^{\mathrm{un}})=-1$, in agreement with the RG calculations in Ref. [13]. Here, the superscripts "co" and "un" are for constrained and unconstrained systems, respectively. However, for a general tricritical system, it was predicted [14] that, in addition to the relation $\alpha^{\mathrm{co}}=-\alpha^{\mathrm{un}}/(1-\alpha^{\mathrm{un}})$, other cases can occur, depending on the relative magnitude of the leading and subleading thermal exponents $y_{t1}$ and $y_{t2}$ and the spatial dimensionality $d$.

In order to verify these theoretical predictions, the present paper presents a more extensive study of constrained tricritical phenomena in two dimensions. The systems investigated include the BC model [15,16], Baxter's hard-square model [17,18], and the $q=1$, 3, and 4 Potts models with vacancies [19]. In comparison with the three-dimensional case, the investigation of two-dimensional systems has some advantages. First, Monte Carlo simulations can be performed for larger linear systems sizes. Second, the tricritical points of the tricritical $q=1$ Potts model and Baxter's hard-square lattice gas are exactly known, and those of the other systems have been determined with a precision in the sixth or seventh decimal place. In contrast, for the three-dimensional BC model, the error estimation of the tricritical point is so far restricted to the fourth decimal place [14]. Third, Baxter's hard-square lattice gas [17,18] is in the same universality class as the tricritical Blume-Capel model, so that the two models can serve for independent tests.

The outline of the remaining part of this paper is as follows. Section II reviews the models, the sampled quantities, and the geometric cluster algorithm, which plays an important role in the present investigation. In Sec. III, we apply the Fisher renormalization mechanism in the generalized context of tricritical scaling. Numerical results are presented in Sec. IV, and a brief discussion is given in Sec. V.

## II. MODELS, SIMULATIONS, AND SAMPLED QUANTITIES

### A. Models

*The Blume-Capel model.* In the development of the theory of tricritical phenomena, the spin-1 model known as the BC model has provided the foundation. The model was independently introduced by Blume [15] and Capel [16]. The reduced Hamiltonian reads

$$\mathcal{H}/k_{\mathrm{B}}T=-K\sum_{\langle i,j\rangle}s_i s_j+D\sum_k s_k^2 \quad (s=0,\pm 1). \tag{3}$$

This Hamiltonian is identical to Eq. (1) when the vector order parameter $\vec{s}$ is replaced by a scalar $s$. Further, in three dimensions, the phase diagram of Eq. (3) is analogous to that of the dilute $XY$ model (1). The universal tricritical exponents of the two-dimensional BC model (3) are known from exact solutions [17,18]; they can also be calculated in the context of the Coulomb gas theory [20,21] and are included in the predictions of conformal field theory [22,23]. The leading and subleading thermal exponents are $y_{t1}=9/5$ and $y_{t2}=4/5$, and the magnetic ones are $y_{h1}=77/40$ and $y_{h2}=9/8$, respectively. Using a sparse transfer-matrix technique and the finite-size scaling, we have located [24] the tricritical point of the square-lattice BC model as $K_t=1.643\,175\,9(1)$ and $D_t=3.230\,179\,7(2)$; the tricritical vacancy density is $\rho_t=0.454\,950\,6(2)$. These results are based on the requirement that both the leading magnetic and energy-energy correlation lengths simultaneously reach their theoretical values. They are consistent with the existing estimate $K_t=1.64(2)$ and $D_t=3.22(4)$ [25], and the precision is considered to be sufficient in the present investigation.

*Baxter's hard-square model.* We also investigate Baxter's tricritical hard-square lattice gas [17,18], which belongs to the same universality class as the tricritical BC model. The Hamiltonian of a general lattice gas on the square lattice can be written as

$$\mathcal{H} = -K\sum_{\langle nn\rangle} \sigma_i\sigma_j - J\sum_{\{nnn\}} \sigma_k\sigma_l + D\sum_k \sigma_k, \tag{4}$$

where $\sigma=0,1$ represents the absence and presence of a particle, respectively. The sums $\langle nn\rangle$ and $\{nnn\}$ are over nearest-neighbor and second-nearest-neighbor sites, respectively. For the hard-square lattice gas, it is required that $K\to-\infty$; i.e., the particles have a "hard"-core so that nearest-neighbor sites cannot be occupied *simultaneously.* For this case, the tricritical point is exactly known [17,18]: $J_t=\ln(3+\sqrt{5})$ and $D_t=\ln[8(1+\sqrt{5})]$. The corresponding vacancy density is $\rho_t=(5+\sqrt{5})/10$.

*The tricritical $q=3$ Potts model.* Just as the tricritical BC model, the tricritical $q=3$ Potts model [19] can be obtained by including vacancies in the "pure" $q=3$ Potts model. The Hamiltonian of such a dilute $q$-state Potts model then reads

$$\mathcal{H} = -K\sum_{\langle nn\rangle} \delta_{\sigma_i,\sigma_j}(1-\delta_{\sigma_i,0}) - D\sum_k \delta_{\sigma_i,0} \quad (\sigma=0,1,\ldots,q), \tag{5}$$

where the lattice site is occupied by a Potts variable $\sigma=1,\ldots,q$ or by a vacancy $\sigma=0$. Nonzero couplings $K$ occur only between nonzero Potts variables. For $q<4$, the phase diagram in the $(K,D)$ plane resembles that of the BC model: a tricritical point occurs between the continuous and the first-order line of transitions. At the tricritical point $(K_t,D_t)$, the critical exponents are [20–23] $y_{t1}=12/7$, $y_{t2}=4/7$, and $y_{h1}=40/21$. Also for this model we used the sparse transfer-matrix method to locate [24] the tricritical point: $K_t=1.649\,913(5)$, $D_t=3.152\,173(10)$, with a corresponding vacancy density $\rho_t=0.345\,72(5)$.

*The dilute $q=4$ Potts model.* The $q=4$ Potts model is a marginal case [19], since the subleading leading thermal exponent satisfies $y_{t2}=0$. The leading thermal and magnetic exponents are [21,22] $y_{t1}=3/2$ and $y_{h1}=15/8$, respectively. The phase transition of a pure Potts model with $q>4$ is of the first-order type [17]. We investigate the dilute $q=4$ Potts model at the point where the leading and subleading thermal fields vanish. We have located [24] this "fixed" point as $K_t=1.457\,90(1)$, $D_t=2.478\,44(2)$, and the corresponding vacancy density is $\rho_t=0.212\,07(2)$.

*The tricritical $q=1$ Potts model.* It has already been known for a long time [26] that the tricritical $q=1$ Potts model is equivalent to the critical Ising model. The Ising clusters of the critical Ising model, a group of spins connected by bonds between equal nearest-neighbor spins, are described by the magnetic exponent of the tricritical $q=1$ Potts model. Here, we shall illustrate this equivalence, starting from the dilute $q$-state Potts model (5), which, for the case $q=1$, simplifies as

$$\mathcal{H} = -K\sum_{\langle nn\rangle} \sigma_i\sigma_j + D\sum_k \sigma_k \quad (\sigma=0,1). \tag{6}$$

For $D\to-\infty$, the vacancies are excluded, and the random-cluster representation describes the "pure" bond-percolation problem. Thus, the random-cluster representation of Eq. (6) corresponds with a mixed-site–bond-percolation model. Because of the attraction between the nonvacancies, this dilute model is different from the conventional site–bond-percolation model [27], in which the vacancies are randomly distributed over the lattice; i.e., different sites are *uncorrelated.* Nevertheless, in general, one expects that the dilute $q\to1$ Potts model, described by Eq. (6), is still in the percolation universality class, and the question arises if it has a tricritical point. The answer follows after substituting the relation $\sigma=(s+1)/2$ in Eq. (6). Apart from a constant, the Hamiltonian (6) reduces to the Ising model in a magnetic field:

$$\mathcal{H} = -K^{(\mathrm{I})}\sum_{\langle nn\rangle} s_is_j - H\sum_k s_k \quad (s_i=\pm1), \tag{7}$$

with the relations

$$K^{(\mathrm{I})}=K/4 \quad H=-D/2+zK/4, \tag{8}$$

where $z$ is the lattice coordination number. Thus, the Ising critical point at $K_c^{(\mathrm{I})}$ and $H=0$ appears in the dilute $q\to1$ Potts model (6) at $K_t=4K_c^{(\mathrm{I})}$ and $D_t=2zK_c^{(\mathrm{I})}$. Since the critical singularity is not percolation like, this point qualifies as the tricritical point of the $q\to1$ Potts model. The spin-up–down symmetry of the critical Ising model yields the vacancy density of the dilute Potts model $\rho_t=1/2$ at tricriticality. Relation (8) shows that the temperaturelike parameters $K$ and $D$ contribute to $K^{(\mathrm{I})}$ and $H$ in the Ising model. Therefore, the leading and subleading thermal exponents of the two-dimensional tricritical $q=1$ Potts model simply follow as

$$y_{t1}=y_h^{(\mathrm{I})}=15/8, \quad y_{t2}=y_t^{(\mathrm{I})}=1. \tag{9}$$

The leading magnetic exponent of the two-dimensional tricritical $q=1$ Potts model is $y_{h1}=187/96$ [26].

### B. Monte Carlo methods

The Hamiltonian for the $q$-state Potts model remains invariant under a global permutation of two of the $q$ Potts states. Thus, one can apply the conventional Swendsen-Wang [28] and Wolff [29] cluster algorithms to simulate these models. However, for most tricritical models defined above (except for the tricritical $q=1$ Potts model), these cluster algorithms are apparently not suitable or sufficient, since they do not operate on the vacancies. For unconstrained systems, a simple solution is to combine these conventional algorithms and the Metropolis method. However, the problem arises as to what sort of Monte Carlo algorithm is appropriate for constrained systems. In principle, one can apply a Kawasaki-like Monte Carlo method [30], which is particle conserving. Unfortunately, this method suffers from a serious critical slowing down, and thus simulations are restricted to small system sizes. This may be one of the reasons why the number of numerical investigations in this subject is rather limited.

In the present work, we make use of the so-called geometric cluster method [31–33], which is developed on the basis of spatial symmetries, such as invariance under the spatial inversion and rotation operations. This algorithm moves groups of spins and particles or vacancies over the lattice in accordance with the Boltzmann distribution, so that the total numbers of spins and particles and vacancies are conserved. It has been shown [31–33] for several models that the percolation threshold of the geometric clusters coincides with the phase transitions, so that the critical slowing down is effectively suppressed.

Then, the constraint is fully realized by a combination of the Wolff and geometric cluster methods, of which the former flips between variables in different Potts states. A particular feature of such constrained simulations is that they *hardly* suffer from a critical slowing down even near tricriticality.

### C. Sampled quantities

*Conventional quantities.* During Monte Carlo simulations, we sampled several quantities, including the moments of the order parameter, the energy density, etc. The magnetic susceptibility is then obtained from the fluctuations of the order parameter $m$ as $\chi=L^2\langle m^2\rangle$. For the BC model (1), $m$ is just the magnetization density; for Baxter's hard-square lattice gas, $m$ is the difference of the vacancy densities on the two sublattices of the square lattice—i.e., $m=\rho^{(1)}-\rho^{(2)}$; and for the tricritical $q=3$ and 4 state Potts models, we define $m^2=\frac{1}{2}\Sigma_{i\neq j}(\rho_i-\rho_j)^2$ where $\rho_i$ is the density of the $i$th Potts state. An energylike quantity $e$ was sampled as nearest-neighbor correlations for the BC and the $q=1$, 3, and 4 state Potts models with vacancies. For Baxter's hard-square lattice gas, the nearest-neighbor sites cannot be occupied simultaneously, so that we sampled $e$ as next-nearest-neighbor correlations. On this basis, a specific-heat-like quantity is defined as $C=L^2(\langle e^2\rangle-\langle e\rangle^2)$, which is proportional to the second derivative of the reduced energy with respect to the coupling constant $K$. Moreover, we sampled energy-energy correlations $g_e(r)=\langle e_0 e_r\rangle-\langle e\rangle^2$. For a lattice with linear system size $L$, the distance $r$ was taken as the half-diagonal distance—i.e., $r=\sqrt{2}L/2$. Since the vacancy density $\rho$ also behaves energy like, we define a compressibilitylike quantity $P=L^2(\langle\rho^2\rangle-\langle\rho\rangle^2)$, which is expected to behave analogously as $C$.

In Monte Carlo studies of critical phenomena, the universal Binder ratio [34] plays a useful role. Thus, we sampled several dimensionless quantities as

$$Q_m=\frac{\langle m^2\rangle^2}{\langle m^4\rangle},\quad Q_e=\frac{\langle(e-\overline{e})^2\rangle^2}{\langle(e-\overline{e})^4\rangle},\quad Q_\rho=\frac{\langle(\rho-\overline{\rho})^2\rangle^2}{\langle(\rho-\overline{\rho})^4\rangle},\tag{10}$$

where $\overline{e}=\langle e\rangle$ and $\overline{\rho}=\langle\rho\rangle$.

*Structure factors.* Apart from the singular behavior of physical observables, a second-order phase transition is generally accompanied by long-range correlations in time and space, and thus large-scale spatial fluctuations exist for the physical observables, such as the magnetization density $m$ and the energy density $e$. It is thus justified to investigate the influence of the constraint on these spatial fluctuations. For this purpose, we define a set of quantities on the basis of spatial inhomogeneities of the magnetization, the energy, and the vacancy density. Consider the Fourier expansion of the order parameter $m(x,y)$ for a system of size $L$:

$$m_{k,l}=\frac{1}{L^2}\int_0^L dx\,dy\,m(x,y)\exp[2\pi i(xk+yl)/L].\tag{11}$$

Obviously, $m_{0,0}$ is just the global magnetization density $m$, and the magnetic susceptibility is $\chi=L^2\langle m^2\rangle=L^2\langle m_{0,0}^2\rangle$; the number $m_{k,l}$ ($k\neq 0$ or $l\neq 0$) represents the spatial inhomogeneity of $m(x,y)$. Since we are especially interested in fluctuations on the largest scales, we define a susceptibilitylike quantity $\chi_s$ in terms of $m_{k,l}$ for the smallest wave numbers:

$$\chi_s=L^2\langle m_{-1,0}m_{1,0}+m_{0,-1}m_{0,1}\rangle=L^2\langle m_s^2\rangle,\tag{12}$$

where, for later convenience, a quantity $m_s$ has been introduced. We shall refer to $\chi_s$ as the structure factor of the susceptibility $\chi$.

Analogously, we sampled the structure factor of the specific heat $C$ as $C_s=L^2\langle e_{-1,0}e_{1,0}+e_{0,-1}e_{0,1}\rangle=L^2\langle e_s^2\rangle$ and that of the compressibility $P$ as $P_s=L^2\langle\rho_{-1,0}\rho_{1,0}+\rho_{0,-1}\rho_{0,1}\rangle=L^2\langle\rho_s^2\rangle$, where $e_{k,l}$ and $\rho_{k,l}$ are obtained from Fourier expansions of the energy and the vacancy density, $e(x,y)$ and $\rho(x,y)$, respectively. On this basis, we sampled the dimensionless ratios

$$Q_{sm}=\frac{\langle m_s^2\rangle^2}{\langle m_s^4\rangle},\quad Q_{se}=\frac{\langle e_s^2\rangle^2}{\langle e_s^4\rangle},\quad Q_{s\rho}=\frac{\langle\rho_s^2\rangle^2}{\langle\rho_s^4\rangle}.\tag{13}$$

The physical meaning of these structure factors can be gleaned from a comparison with the conventional quantities. For instance, both $\chi$ and $\chi_s$ represent fluctuation strengths of the order parameter $m$ and can be expressed in terms of a summation involving the magnetic correlation function, whose scaling behavior is described by the correlation function exponents $\eta$ and $\nu$. Thus, we expect that, in unconstrained systems, the structure factors $\chi_s$, $C_s$, and $P_s$ display the same scaling behavior as $\chi$, $C$, and $P$, respectively. However, as we shall see, there are interesting differences in constrained systems.

## III. FINITE-SIZE SCALING BEHAVIOR IN CONSTRAINED SYSTEMS

A finite-size analysis of constrained phenomena precisely at tricriticality has recently been reported [14]. This analysis follows the basic idea of the Fisher renormalization mechanism, which has been formulated for *critical* systems [6]. In this section, we shall briefly review and moreover generalize the procedures in Ref. [14], such that we can also account for the constrained scaling behavior due to deviations from the tricritical vacancy density.

As a first step, we express the finite-size scaling formula of the reduced free energy near tricriticality as

$$f(t_1,t_2,L) = L^{-d} f_s(L^{y_{t1}} t_1, L^{y_{t2}} t_2, 1) + f_a(t_1,t_2), \qquad (14)$$

where $t_1$ and $t_2$ are the leading and subleading thermal fields, respectively. In the language of the BC model, $t_1$ and $t_2$ are analytic functions of the coupling constant $K$ and the chemical potential $D$. The symbols $f_s$ and $f_a$ are the singular and analytical parts of the free energy, respectively. The expectation value of vacancy density $\langle\rho\rangle$ follows by differentiation as

$$-\langle\rho(t_1,t_2)\rangle = \frac{\partial f}{\partial D} = a_1 L^{y_{t1}-d} f_s^{(1,0)}(t_1 L^{y_{t1}}, t_2 L^{y_{t2}}) + a_2 L^{y_{t2}-d} f_s^{(0,1)} \times (t_1 L^{y_{t1}}, t_2 L^{y_{t2}}) + a_1 f_a^{(1,0)}(t_1,t_2) + a_2 f_a^{(0,1)}(t_1,t_2), \qquad (15)$$

where $a_1 = \partial t_1 / \partial D$ and $a_2 = \partial t_2 / \partial D$ are constants. The superscripts $(i,j)$ represent $i$ differentiations with respect to $t_1$ and $j$ differentiations to $t_2$. Linearization at the tricritical point yields

$$-\delta\rho = b_1 L^{2y_{t1}-d} t_1 + b_2 L^{y_{t1}+y_{t2}-d} t_2 + b_3 t_1 + b_4 t_2 + \cdots, \qquad (16)$$

where $b_1$, $b_2$, $b_3$, and $b_4$ are constants and $\delta\rho = \langle\rho(t_1,t_2)\rangle - \langle\rho(0,0)\rangle$ is the deviation of the vacancy density from its tricritical value. The constraint that the vacancy density be fixed at the tricritical value yields $\delta\rho = 0$ in Eq. (16). As a consequence, the thermal fields $t_1$ and $t_2$ are related, but in a way which still depends on which terms in the right-hand side of Eq. (16) dominate. We consider the case of large $L$ and then distinguish three cases:

(i) For $2y_{t1} - d > 0$ and $y_{t1} + y_{t2} - d > 0$, one has $L^{y_{t1}} t_1 \propto L^{y_{t2}} t_2$—i.e., $t_2 \gg t_1$ and $K - K_{tc} \simeq t_2$—so that the leading thermal exponent of the constrained systems is equal to the subleading exponent $y_{t2}$.

(ii) For $2y_{t1} - d > 0$ but $y_{t1} + y_{t2} - d < 0$, one has $L^{y_{t1}} t_1 \propto L^{d-y_{t1}} t_2$. The leading thermal exponent is thus renormalized as $y_{t1} \to d - y_{t1}$. Again, we have $t_2 \gg t_1$ and $K - K_{tc} \simeq t_2$.

(iii) For $2y_{t1} - d < 0$—i.e., the unconstrained specific heat does not diverge at tricriticality—$t_1$ is approximately proportional to $t_2$ and no exponent renormalization occurs.

Therefore, for a tricritical system with a divergent specific heat ($2y_{t1} - d > 0$), the leading thermal exponent $y_{t1}$ is renormalized to $d - y_{t1}$ under the constraint, while the subleading one remains unchanged. Thus, the finite-size scaling relation for the difference of $K$ to the tricritical point is $(K - K_t) \to (K - K_t) L^{d-y_{t1}} + a_0 (K - K_t) L^{y_{t2}}$, with $a_0$ a constant.

Next, we consider the case that the fixed vacancy density $\rho$ differs slightly from the tricritical value $\rho_t$—i.e., $\delta\rho = \rho - \rho_t \neq 0$ in Eq. (16). We first consider cases (i) and (ii)—i.e., $2y_{t1} - d > 0$. We rewrite Eq. (16) as

$$L^{y_{t1}} t_1 = -b_1^{-1} [(\delta\rho + b_4 t_2) L^{d-y_{t1}} + b_2 t_2 L^{y_{t2}} + \cdots], \qquad (17)$$

where we have omitted the term with amplitude $b_3$ which contributes a smaller power of $L$ than the left-hand side. After substitution in Eq. (14), neglecting less relevant terms, we obtain

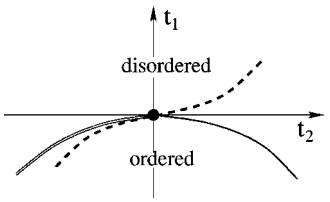


FIG. 1. Illustration of the application of the Fisher renormalization mechanism to tricritical systems. The tricritical point $(K_t, D_t)$ is denoted as the black circle, and the solid single and double lines represent the critical and first-order-transition lines, respectively. The variables $t_1$ and $t_2$ are the leading and subleading thermal fields at the tricritical point, respectively. The constraint that the vacancy density $\rho$ is fixed at the tricritical value $\rho_t$ is described by the dashed line, part of which coincides with the first-order transition line. As a consequence of the constraint, the scaling fields $t_1$ and $t_2$ are related, and this relation is singular at tricriticality.

$$f(t_1,t_2,L) = L^{-d} f_s(-b_1^{-1} L^{d-y_{t1}} (\delta\rho + b_4 t_2) - (b_2/b_1) L^{y_{t2}} t_2, L^{y_{t2}} t_2, 1) + f_a(0,t_2), \qquad (18)$$

which can be written more simply as

$$f(t_1,t_2,L) = L^{-d} f_s'(L^{d-y_{t1}} t_1', L^{y_{t2}} t_2) + f_a(0,t_2), \qquad (19)$$

where $t_1' \equiv \delta\rho + b_4 t_2$. This means that the deviation $(\rho - \rho_t)$ from the tricritical density combines with $t_2$ to act as a scaling field with a renormalization exponent $d - y_{t1}$; i.e., the finite-size effect of this linear combination is multiplied by $L^{d-y_{t1}}$.

In the constrained system, we wish to express the constrained free energy in $K$ and $\rho$ instead of $t_2$ and $\rho$. In cases (i) and (ii), the constraint equation (16) shows that $t_1 \ll t_2$ for large $L$. Since $t_1$ and $t_2$ are written as linear combinations of $K$ and $D$, we may write $K - K_t \simeq t_2$ apart from corrections with negative powers of $L$. Thus we have

$$t_1' = \delta\rho + \alpha(K - K_t), \quad t_2 = K - K_t. \qquad (20)$$

Then, the scaling behavior of constrained quantities can be obtained from differentiations of Eq. (19) with respect to appropriate scaling fields.

For case (iii), no exponent renormalization occurs and $\delta\rho$ approaches a linear combination of $t_1$ and $t_2$; i.e., the distance $\rho - \rho_t$ behaves in leading order as the scaling fields $t_1$ and $t_2$, independent of $L$.

The essential element of the above procedure is the solution of the constraint equation $\delta\rho = \text{const}$ in terms of a relation between $K$ and $D$. In the parameter space $(t_1, t_2)$, this solution is sketched in Fig. 1. The path of the constrained system, the dashed line, is singular at tricriticality, and for the case $2y_{t1} - d > 0$, renormalization of critical exponents occurs.

As mentioned earlier, in addition to uniform fluctuations, a second-order phase transition is also accompanied by inhomogeneous large-scale spatial fluctuations. Without the constraint, these two types of fluctuations display the same scaling behavior. However, their behavior becomes qualitatively different in constrained systems when the uniform fluctuations are sufficiently strongly suppressed by the constraint. A

good test for such a difference is to compare the critical behavior of the structure factors $\chi_s$, $C_s$, and $P_s$ with $\chi$, $C$, and $P$, respectively. According to Eq. (19), the exponents describing the behavior of $C$ and $P$ are modified as long as $2y_{t1}-d>0$. In contrast, since the constraint does not lead to a change of the universality class, one may expect that the leading finite-size scaling behavior of $C_s$ and $P_s$ remains unchanged at tricriticality. This will be confirmed by our numerical data later.

We conclude this section by pointing out the following implicit assumption. In the derivation of Eq. (16), we require that the expectation value $\langle\rho\rangle$ of the vacancy density be a constant, while, in fact, we should require that $\rho$ itself is a constant. For $L\to\infty$, no difference exists between $\langle\rho\rangle$ and $\rho$. In a finite system, however, $\rho$ need not be equal to $\langle\rho\rangle$; i.e., fluctuations of the vacancy density are allowed even if $\langle\rho\rangle$ is a constant. As mentioned earlier, the Monte Carlo simulations to be performed in this work conserve the number of vacancies, which leads to a "stronger" constraint than $\langle\rho\rangle$ =(const). Thus, the application of the Fisher renormalization mechanism in this paper used the assumption that suppressing the fluctuations of $\rho$ about $\langle\rho\rangle$ does not lead to a qualitative change in the leading scaling behavior of the constrained system.

## IV. RESULTS

### A. Tricritical $q=1$ Potts model

The tricritical $q=1$ Potts model is particularly suitable to illustrate the Fisher renormalization mechanism for constrained tricritical phenomena. The equivalence of this model with the Ising model in a magnetic field, as mentioned in Sec. II, makes it possible to use the known properties of the latter model, and thus there is no obvious need for simulations. The energy density and the specific heat in the two models are related as

$$\langle e\rangle \propto \langle e^{(\mathrm{I})}\rangle + 2\langle m^{(\mathrm{I})}\rangle, \quad C \propto C^{(\mathrm{I})} + 4\chi^{(\mathrm{I})}, \tag{21}$$

where the superscript (I) is for the Ising model. Thus, the leading behavior of the Potts specific heat $C$ is just that of the Ising magnetic susceptibility $\chi^{(\mathrm{I})}$. This illustrates the fact that the leading $q=1$ Potts tricritical thermal exponent $y_{t1}$ is equal to the magnetic exponent $y_h^{(\mathrm{I})}$ of the Ising model. However, the leading scaling behavior of $\langle e\rangle$ of the Potts model (6) is "accidentally" governed by the exponent $y_t^{(\mathrm{I})}$, the subleading Potts thermal exponent $y_{t2}$. This is due to the symmetry between plus and minus Ising spins.

The dilute $q=1$ Potts model with its vacancy density $\rho$ fixed at $\rho_t=1/2$ is equivalent to an Ising model with zero magnetization. Thus, the constrained susceptibility $\chi^{(\mathrm{I})}$ vanishes in Eq. (21), and the Potts and Ising specific heats $C$ and $C^{(\mathrm{I})}$ become identical. Further, the constraint on the Ising model is of the magnetic type, so that the scaling behavior of $C^{(\mathrm{I})}$ is not qualitatively influenced. Thus, one can conclude that, under the constraint, the Potts specific heat $C$ is governed by the second thermal exponent $y_{t2}$—i.e., the Ising thermal exponent $y_t^{(\mathrm{I})}=1$. This is as predicted in Sec. III for the case $2y_{t1}-d>0$, $y_{t1}+y_{t2}-d>0$.

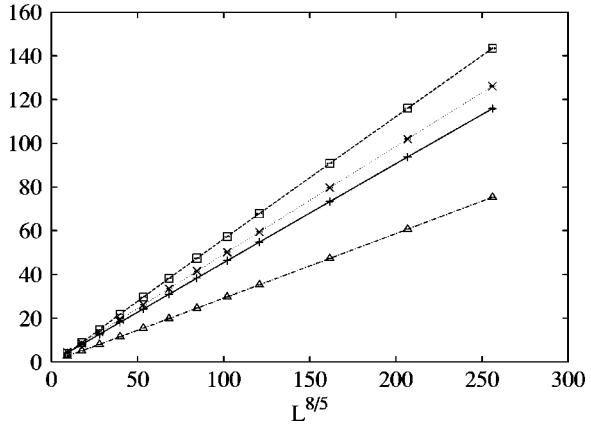


FIG. 2. Specific-heat-like quantities in the unconstrained BC model at tricriticality vs $L^{8/5}$. These quantities include $C/10$(+), $2P$(×), $C_s$(□), and $10P_s$(△). The approximate linearity of the data illustrates that the leading behavior of these quantities is governed by the exponent $2y_{t1}-2$, with $y_{t1}=9/5$.

### B. Tricritical Blume-Capel model

#### 1. Unconstrained systems

For the unconstrained tricritical systems in the present paper, the nature of the critical behavior is now well established [20,21]. The finite-size expression of the reduced free energy is given by Eq. (14), and the scaling behavior of the aforementioned conventional quantities is obtained by differentiating Eq. (14) with respect to appropriate scaling fields. These quantities include the energy density $\langle e\rangle$, the specific heat $C$, the magnetic susceptibility $\chi$, the energy-energy correlation function $g_e(r=L/\sqrt{2})$, etc. Precisely at tricriticality, one has

$$\langle e(L)\rangle = e_0 + e_1 L^{y_{t1}-2} + e_2 L^{y_{t2}-2} + \cdots,$$

$$C(L) = c_0 + c_1 L^{2y_{t1}-2} + c_2 L^{y_{t1}+y_{t2}-2} + c_3 L^{2y_{t2}-2} + \cdots,$$

$$P(L) \propto C(L),$$

$$\chi(L) = \chi_0 + \chi_0 L^{2y_{h1}-4} + \cdots,$$

$$g_e(L) = g_1 L^{2y_{t1}-4} + g_2 L^{y_{t1}+y_{t2}-4} + \cdots. \tag{22}$$

The constants, $e_0$, $c_0$, and $\chi_0$, arise from the analytic part of the free energy density. As discussed above, we expect that the structure factors $C_s$, $P_s$, and $\chi_s$ behave in a similar way as the physical quantities $C$, $P$, and $\chi$, respectively.

For a comparison with constrained phenomena investigated later, we simulated the tricritical BC model on the square lattice precisely at the tricritical point [24] $K_t$ =1.643 175 9(1) and $D_t$=3.230 179 7(2). The Monte Carlo simulations used a combination of Metropolis and Wolff steps, which allows fluctuations of the magnetization as well as the density of the vacancies. Periodic boundary conditions were applied, and the system sizes were taken in the range $4\leqslant L\leqslant 32$. The Monte Carlo data for $C$, $P$, $C_s$, and $P_s$ are shown versus $L^{8/5}$ in Fig. 2. The approximate linearity of these data lines indicates that all these quantities are specific

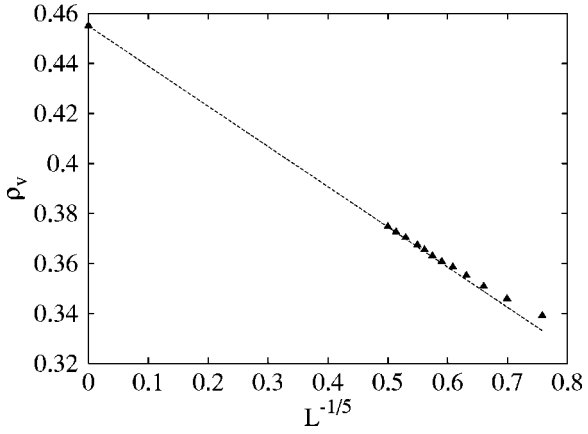


FIG. 3. Vacancy density $\rho$ of the unconstrained BC model at tricriticality vs $L^{y_{t1}-2}=L^{-1/5}$. As expected, the vacancy density $\rho$ is an energylike quantity.

heat like; the scaling behavior is described by Eq. (22) with the exponent $y_{t1}=9/5$. Further, we observed that $\chi \propto \chi_s \propto L^{2y_{h1}-2}=L^{37/20}$ (not shown). The data for the vacancy density $\rho$ is shown versus $L^{y_{t1}-2}=L^{-1/5}$ in Fig. 3, where we include the $L\to\infty$ tricritical value $\rho_t=0.454\,950\,6(2)$, taken from Ref. [24].

For the universal ratios defined in Sec. II including $Q_m$, $Q_e$, $Q_\rho$, $Q_{sm}$, $Q_{se}$, and $Q_{s\rho}$, we fitted the data according to the least-squares criterion by

$$Q(L) = Q + b_1 L^{y_i} + b_2 L^{2y_i}, \tag{23}$$

where the terms with amplitudes $b_1$ and $b_2$ account for corrections with the irrelevant scaling exponent $y_i=-1$ for the $q=2$ Potts tricritical universality class in two dimensions [17,18,21,22]. The results, shown in Table I, indicate that the universal asymptotic values of $Q_e$ and $Q_{se}$ are identical to those of $Q_\rho$ and $Q_{s\rho}$, respectively. This is as expected, since both $\langle e\rangle$ and $\rho$ are energy like.

#### *2. Constrained systems*

Simulations of the constrained BC model used a combination of Wolff and geometric cluster steps, as discussed earlier. Periodic boundary conditions were used, and the system sizes were taken in the range $6\leqslant L\leqslant 720$. For each system size, about $5\times 10^7$ samples were taken.

*Constrained behavior at the tricritical point.* The tricritical point was taken from Ref. [24] as $K_t=1.643\,175\,9(1)$, $\rho_t=0.454\,950\,6(2)$. For a finite system $L$, however, the total number of vacancies, $V_t=L^2\rho_t$, is generally not an integer. In that case, the actual simulations were performed at $V_-=[V_t]$ and $V_+=[V_t+1]$, where brackets [] denote the integer part. For a sampled quantity $A$, its tricritical value $A_t$ is then obtained by a linear interpolation as $A_t=xA_+ +(1-x)A_-$, with $x=V_t-V_-$; the statistical error margin of $A_t$ is estimated as $\delta A_t=\sqrt{(x\,\delta A_+)^2+[(1-x)\,\delta A_-]^2}$. The data for the constrained specific heat $C$ and the energy density $\langle e\rangle$ are shown in Figs. 4 and 5. In comparison with Figs. 2 and 3, these figures indicate that the scaling behavior of $C$ and $\langle e\rangle$ is indeed modified by the constraint. In particular, the constrained specific heat $C$ reaches only a finite value instead of being divergent for $L\to\infty$. The exponents used for the horizontal axes in Figs. 4 and 5 are those predicted in Sec. III. For the tricritical BC model in two dimensions, the Fisher mechanism predicts that the leading thermal singularity in constrained system is determined by the subleading exponent $y_{t2}$, because the renormalized exponent $2-y_{t1}=1/5$ is smaller than $y_{t2}=4/5$. Thus, one obtains the leading finite-size behavior $\langle e\rangle \propto L^{y_{t2}-2}=L^{-6/5}$ and $C\propto L^{2y_{t2}-2}=L^{-2/5}$, in agreement with Figs. 4 and 5, respectively. By differentiating Eq. (19) with respect to the thermal fields $\tau_1$ and $\tau_2$, the finite-size dependence of $C$ and $\langle e\rangle$ follows as

$$C = c_0 + a_1 L^{2y_{t2}-2} + a_2 L^{y_{t2}-y_{t1}} + a_3 L^{2-2y_{t1}} + \cdots,$$

$$\langle e\rangle = e_0 + b_1 L^{y_{t2}-2} + b_2 L^{-y_{t1}} + \cdots, \tag{24}$$

where the constants $c_0$ and $e_0$ are equal to those in Eq. (22). The $\langle e\rangle$ and $C$ data were fitted by Eq. (24), with $y_{t1}$ fixed at $9/5$. In order to obtain a satisfactory fit, the data for small system sizes $L\leqslant 8$ were discarded. We obtain $y_{t2}=0.798(4)$ and 0.803(4) from the fit of $C$ and $\langle e\rangle$, respectively. These results are in good agreement with the exact value $y_{t2}=4/5$.

The $g_e(r)$ data for $r=\sqrt{2}L/2$ at tricriticality are shown in Fig. 6. The approximate linearity indicates that the scaling behavior of $g_e$ is still governed by the leading thermal exponent $y_{t1}$—i.e., $g_e\propto L^{2y_{t1}-4}=L^{-2/5}$ as described by Eq. (22). This confirms that, as expected, the power law describing the spatial correlations is not affected by the constraint, although the amplitude become negative. For an illustration of the influence of the constraint on inhomogeneous fluctuations, we sampled the structure factors $C_s$ and $P_s$, which display the same scaling behavior as $C$ and $P$ in the unconstrained systems, as shown in Fig. 2. The constrained data for $C_s$ and $P_s$ are shown in Fig. 7. In contrast to the conventional quantities $C$ and $P$, the leading behavior of the tricritical structure factors $C_s$ and $P_s$ *remains the same* as in the unconstrained systems. The numerical data were fitted by Eq. (22) with the exponent $y_{t2}$ fixed at $4/5$. After a cutoff for small systems sizes $L\leqslant 8$, we obtain $y_{t1}=1.799(2)$ and 1.798(2) from the fits for $C_s$ and $P_s$, respectively. These results are in good agreement with the exact value $y_{t1}=9/5$.

TABLE I. Fit results for the dimensionless quantities of the constrained (Constr.) and the unconstrained (Uncon.) Blume-Capel model.

| Quantity | $Q_m$ | $Q_e$ | $Q_\rho$ | $Q_{sm}$ | $Q_{se}$ | $Q_{s\rho}$ |
|---|---|---|---|---|---|---|
| Uncon. | 0.6620(5) | 0.596(2) | 0.597(2) | 0.4349(5) | 0.4720(8) | 0.4705(8) |
| Constr. | 0.9821(1) | 0.3331(2) | — | 0.81222(5) | 0.84810(6) | 0.84804(6) |

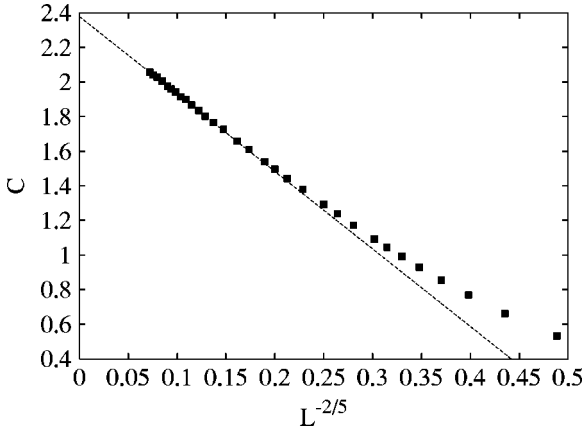


FIG. 4. Specific heat $C$ of the constrained BC model at tricriticality vs $L^{2y_{t2}-2}=L^{-2/5}$. The approximate linearity at the left-hand side implies that $C$ is governed by the subleading thermal exponent $y_{t2}$, as predicted by the Fisher renormalization.

As an illustration of the influence that the energylike constraint has on magnetic quantities, we sampled the quantities $\chi$ and $\chi_s$. The data are shown in Fig. 8, where the exponent $37/20$ used for the horizontal scale is equal to $2y_{h1}-2$ with $y_{h1}=77/40$ [20–22]. Thus, the constraint does not change the leading scaling behavior of magnetic quantities. This is apparently related to the fact that the chemical potential $D$, the conjugate parameter of the vacancy density $\rho$, is not directly coupled to the magnetic field.

The data for the universal ratios, including $Q_m$, $Q_e$, $Q_\rho$, $Q_{sm}$, $Q_{se}$, and $Q_{s\rho}$, were also fitted by Eq. (23). We assume that, under the constraint, finite-size corrections still mainly arise from the irrelevant field. After a cutoff for small system sizes $L\leqslant 10$, satisfactory fits can be obtained. The results are shown in Table I, where the quoted error margins are two statistical standard deviations. Thus, although the dimensionless ratios are universal, they assume different values in unconstrained and constrained systems. The reason is that these ratios depend on the spatial profile of correlation functions. Here the constraint plays a similar role as the boundary conditions, the aspect ratios, etc. A particular feature in Table I is that the constrained ratio $Q_e=0.3331(2)\approx 1/3$. This indicates that the fluctuations of the energy density resemble the normal (Gaussian) distribution. As reflected by the fact that the specific heat $C$ remains finite in constrained systems, this is because singularities of energy-related quantities are strongly suppressed so that the "background" (the analytical part of the free energy) plays an enhanced role.

*Constrained behavior near the tricritical point.* In addition to the tricritical point, the Fisher renormalization mechanism also predicts the scaling behavior as a function of the distances $K-K_t$ and $\rho-\rho_t$. In this case, the dimensionless ratios serve a good choice for such investigations. The $Q_m$ data at $K=K_t$ are partly shown in Fig. 9 as a function the vacancy density. They indicate that the exponent $y_\rho$ of the deviation of the vacancy density $\rho-\rho_t$ is much smaller than 1—i.e., $y_\rho \ll 1$—in agreement with the prediction by Eq. (19). The $Q_m$ data were fitted by

$$Q_m(\rho,L) = Q_m + \sum_{k=1}^{4} a_k(\rho-\rho_t)^k L^{k(2-y_{t1})} + b_1 L^{y_i} + b_2 L^{2y_i} + c_1(\rho-\rho_t)L^{2-y_{t1}+y_i} + c_2(\rho-\rho_t)^2 L^{2-y_{t1}} + \cdots , \tag{25}$$

where the term with $c_1$ describes the "mixed" effect of the leading irrelevant field and the scaling field $\tau_1$ in Eq. (19). The term with $c_2$ arises from the nonlinear dependence of $\tau_1$ on the distance $\rho-\rho_t$. The irrelevant exponent was fixed at $y_i=-1$. Discarding the data for for small system sizes $L \leqslant 12$, we obtain $y_{t1}=1.796(5)$, in agreement with the exact value $y_{t1}=9/5$.

As shown earlier, precisely at the tricritical point, the leading scaling behavior of the structure factors is not renormalized under the constraint. However, we argue here that the constrained scaling behavior of these quantities as a function of the distance to the tricritical point is still governed by Eq. (19). Thus, the leading finite-size scaling of $C(\rho,K,L)$ and $C_s(\rho,K,L)$ can be expressed as

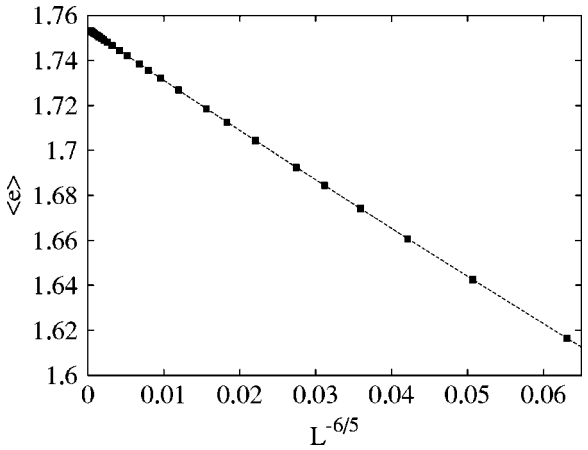


FIG. 5. Energy density $\langle e\rangle$ of the constrained BC model at tricriticality vs $L^{y_{t2}-2}=L^{-6/5}$. The approximate linearity for large $L$ is in agreement with the Fisher renormalization.

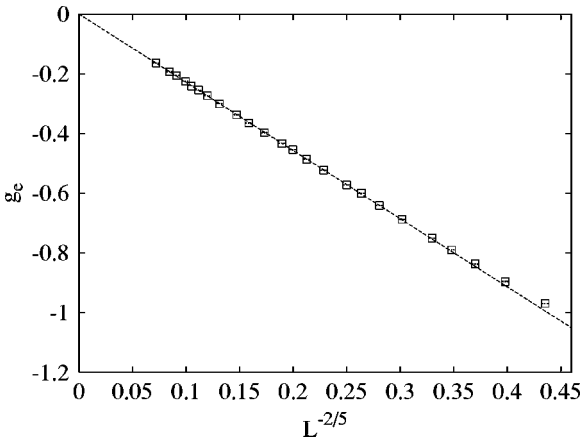


FIG. 6. Energy-energy correlations $g_e(r)$ of the constrained BC model at tricriticality vs $L^{2y_{t1}-4}=L^{-2/5}$. The distance $r$ was taken as $L/\sqrt{2}$, the half-diagonal system size. The approximate linearity indicates that the critical exponent for $g_e(r)$ is not renormalized.

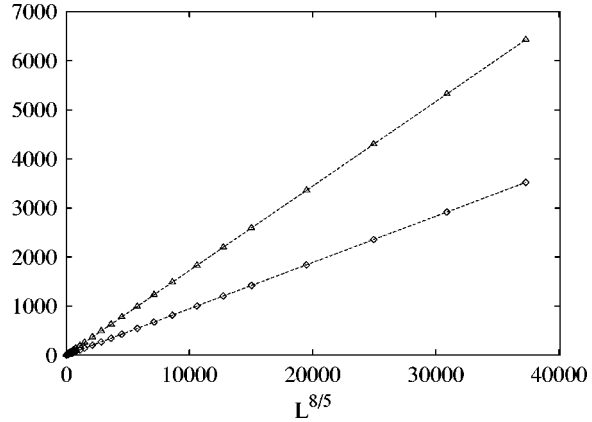


FIG. 7. Structure factors, $C_s/10(\triangle)$ and $P_s(\diamond)$, of the constrained BC model at tricriticality vs. $L^{2y_{t1}-2}=L^{8/5}$. The approximate linearity suggests that the critical exponents for these structure factors are not renormalized.

$$C(\tau_1,\tau_2,L) = c(\tau_1,\tau_2) + L^{2y_{t2}-2}C(\tau_1 L^{2-y_{t1}}, \tau_2 L^{y_{t2}}),$$

$$C_s(\tau_1,\tau_2,L) = c_a(\tau_1,\tau_2) + L^{2y_{t1}-2}C_s(\tau_1 L^{2-y_{t1}}, \tau_2 L^{y_{t2}}), \tag{26}$$

where $\tau_1=(\rho-\rho_t)+a(K-K_t)$ and $\tau_2=(K-K_t)$ act as scaling fields. The terms $c(\tau_1,\tau_2)$ and $c_a(\tau_1,\tau_2)$ arise from the analytical background. For the case $K=K_t$, Taylor expansions of Eq. (26) yield the behavior of $C_s(\rho,L)$ as

$$C_s(\rho,L) = c_{a0} + c_{a1}(\rho-\rho_t) + c_{a2}(\rho-\rho_t)^2 + L^{2y_{t1}-2}\Big[ d_0 + \sum_k a_k(\rho-\rho_t)^k L^{k(2-y_{t1})} + b_1 L^{y_i} + b_2 L^{2y_i}\Big]. \tag{27}$$

We fitted $C_s$ data for $K=K_t$ by Eq. (27). After a cutoff for small system sizes $L\leqslant 10$, we obtain the leading thermal exponent $y_{t1}=1.793(8)\approx 9/5$.

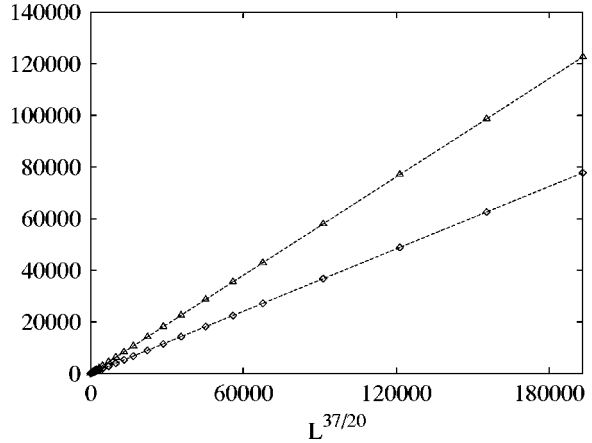


FIG. 8. Susceptibilitylike quantities $\chi/(\square)$ and $\chi_s\times 10(\triangle)$ of the constrained BC model at tricriticality vs $L^{2y_{h1}-2}=L^{37/20}$. The approximate linearities suggest that the constraint does not qualitatively influence the leading scaling behavior of magnetic quantities.

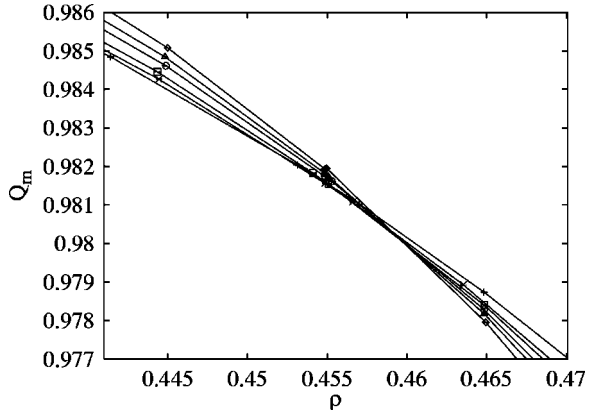


FIG. 9. Dimensionless ratio $Q_m$ of the constrained BC model with $K=K_t$ vs vacancy density $\rho$. The system sizes are $L=16(+)$, 24 $(\times)$, 32 $(\square)$, 48 $(\bigcirc)$, 64 $(\triangle)$, and 96 $(\diamond)$. The small finite-size dependence of the slopes of these curves indicates that the critical exponent governing the scaling behavior of $Q_m$ as a function of $\rho-\rho_t$ is much smaller than 1.

For an infinite system with the coupling constant $K=K_t$, the specific-heat-like quantities $C$ and $C_s$ behave as $C\propto(\rho-\rho_t)^{-\alpha_\rho}$ and $C_s\propto(\rho-\rho_t)^{-\alpha_{s\rho}}$, respectively. The exponents $\alpha_\rho$ and $\alpha_{s\rho}$ can be obtained by regarding $L$ as a scaling factor, which satisfies $(\rho-\rho_t)L^{2-y_{t1}}=1$. From Eq. (26), one simply has $\alpha_\rho=(2y_{t2}-d)/(d-y_{t1})=-2$ and $\alpha_{s\rho}=(2y_{t1}-d)/(d-y_{t1})=8$. Similarly, for the case $\rho=\rho_t$, the specific heat $C$ and the structure factor $C_s$ behave $C\propto(K-K_t)^{-\alpha}$ and $C_s\propto(K-K_t)^{-\alpha_s}$ in an infinite system, respectively. Following the same procedure, one can obtain $\alpha=(2y_{t2}-d)/y_{t2}=-1$ and $\alpha_s=(2y_{t1}-d)/y_{t2}=2$.

As an illustration of the renormalization exponents due to the difference of $K$ to the tricritical point, the $Q_{sm}$ data for $\rho=\rho_t$ are partly shown in Fig. 10 as a function of $K$. We fitted these $Q_{sm}$ data by

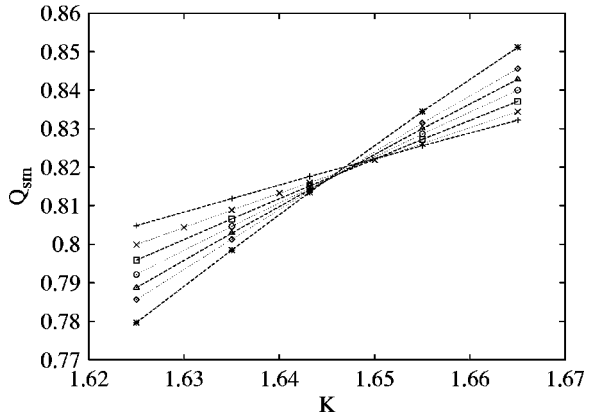


FIG. 10. Dimensionless ratio $Q_{sm}$ of the constrained tricritical BC model at a fixed tricritical vacancy density $\rho=\rho_t$ vs coupling constant $K$. The data points $+$, $\times$, $\square$, $\bigcirc$, $\triangle$, $\diamond$, and * represent $L=24$, 32, 40, 48, 56, 64, and 80, respectively.

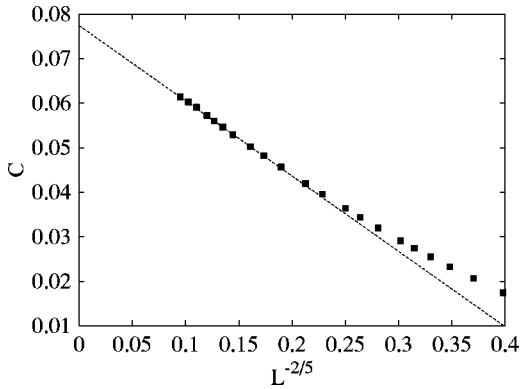


FIG. 11. Constrained specific heat $C$ of Baxter's hard-square lattice gas at tricriticality vs $L^{2y_{t2}-2}=L^{-2/5}$, in agreement with the prediction of the Fisher renormalization.

$$Q_{sm}(K,L) = Q_{sm} + \sum_{k=1}^{4} a_{1k}(K-K_t)^k L^{ky_{t2}} + b_1 L^{y_i} + b_2 L^{2y_i} + c_1(K-K_t)L^{y_{t2}+y_i} + c_2(K-K_t)^2 L^{y_{t2}} + \cdots . \tag{28}$$

The exponent $y_i$ were fixed at $-1$, and the data for small system sizes $L \leqslant 10$ were discarded. We obtain $y_{t2} = 0.806(7)$, in agreement with the exact value $y_{t2} = 4/5$.

### C. Baxter's hard-square model

Within the same universality class of the tricritical BC model, we also investigate Baxter's hard-square lattice gas [17,18], which is described by Eq. (4). Constrained simulations used the geometric cluster algorithm only and took place at the exactly known tricritical point $J_t = \ln(3+\sqrt{5})$ and $\rho_t = (5+\sqrt{5})/10$. We used periodic boundary conditions and 24 system sizes in the range $4 \leqslant L \leqslant 360$. Again, the actual simulations were performed for two integer numbers of vacancies, and the tricritical quantities are obtained by a linear interpolation. This model serves an independent test for the constrained behavior discussed in the above subsection. We observe that, as expected, the constrained tricritical phenomena of this lattice gas and of the BC model are very similar. For instance, the constrained tricritical specific heat of the lattice gas also reaches a finite value as $L^{-2/5}$, illustrated in Fig. 11. For this reason, we do not give a detailed account of the numerical results.

### D. Tricritical $q=3$ Potts model

Using a combination of Metropolis, Wolff, and geometric cluster steps, we first simulated the unconstrained $q=3$ Potts model with vacancies at the tricritical point [24] $K_t = 1.649\,913(5)$ and $D_t = 3.152\,17(1)$. The system sizes were taken in the range $6 \leqslant L \leqslant 32$, and the specific heat $C$ and the energy density $\langle e \rangle$ were sampled. As expected, we found that these data are well fitted by Eq. (22), with the exact thermal exponents $y_{t1} = 12/7$ and $y_{t2} = 4/7$.

Next, we performed constrained simulations at tricriticality using the determined tricritical vacancy density [24] $\rho_t = 0.345\,72(5)$. The system sizes were chosen as 20 values in the range $6 \leqslant L \leqslant 280$. The Monte Carlo data for $C$ and $\langle e \rangle$ are shown in Figs. 12 and 13, respectively. Again, the tricritical specific heat $C$ is suppressed and remains finite under the constraint. These figures confirm that the leading behavior of $C$ and $\langle e \rangle$ is governed by the exponents $2-2y_{t1}$ and $-y_{t1}$, respectively, as predicted by Eq. (24). For a quantitative confirmation, the $C$ data were fitted by Eq. (24). First, we fixed $y_{t1}$ at $12/7$ [20–22]. After discarding the data for small system sizes $L \leqslant 10$, we obtain $y_{t2} = 0.572(3) \approx 4/7$. Next, we fixed $y_{t2}$ at $4/7$ and obtain $y_{t1} = 1.714(2) \approx 12/7$.

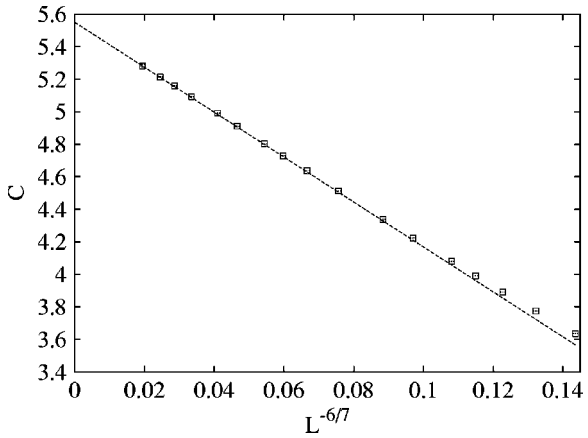


FIG. 12. Constrained specific heat $C$ of the $q=3$ Potts model at tricriticality vs $L^{2y_{t2}-2}=L^{-6/7}$, in agreement with the prediction of the Fisher renormalization.

The scaling behavior of magnetic quantities and the structure factors also remains unchanged under the constraint, as expected. As an illustration, the $C_s$ data are shown in Fig. 14, indicating that at tricriticality $C_s$ diverges indeed as $L^{2y_{t1}-2} = L^{10/7}$.

### E. Dilute $q=4$ Potts model

The $q=4$ Potts model is a marginal case of the tricritical Potts model in the sense that the critical and the tricritical branch merge at $q=4$; accordingly, the subleading thermal

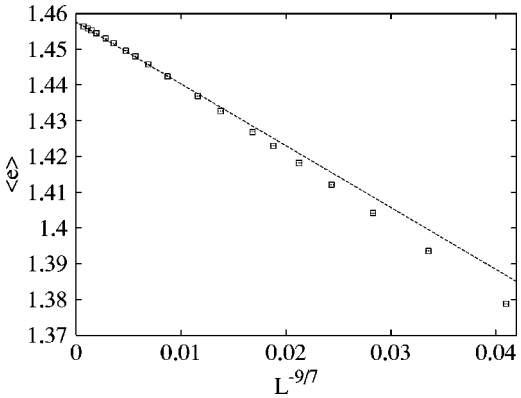


FIG. 13. Energy density $\langle e \rangle$ of the constrained $q=3$ Potts model at tricriticality vs $L^{y_{t2}-2}=L^{-9/7}$, as predicted by the Fisher renormalization.

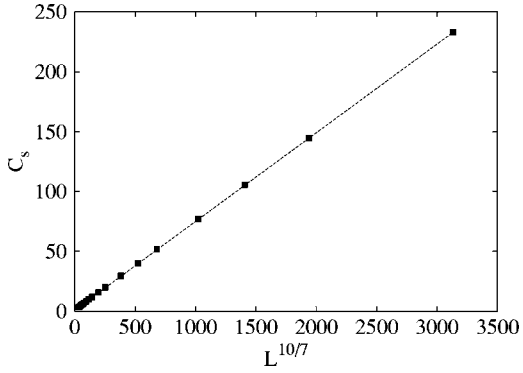


FIG. 14. Structure factor of the specific heat $C_s$ of the constrained $q=3$ Potts model at tricriticality vs $L^{2y_{t1}-2}=L^{10/7}$.

exponent vanishes—i.e., $y_{t2}=0$ [19]. In this case, we expect that the leading thermal exponent in constrained systems is equal to $2-y_{t1}=1/2$. This corresponds with case (ii) in Sec. III. Constrained simulations were performed at the "fixed" point—i.e., $K_t=1.457\,90(1)$ and $\rho_t=0.212\,07(2)$ [24]—where logarithmic corrections due to the marginal field associated with $y_{t2}$ are absent. The system sizes took 20 values in the range $12\leqslant L\leqslant 280$. The $C_s$ data are plotted in Fig. 15. They show no indication that the constraint introduces slowly convergent finite-size corrections. According to Eq. (24), the $C$ and $\langle e\rangle$ data are plotted versus $1/L$ and $L^{-3/2}$ in Figs. 16 and 17, respectively. In contrast to the tricritical systems discussed above, the leading terms in Eq. (24) are insufficient even to approximately describe these numerical data. Remarkably, the energy density $\langle e\rangle$ has a maximum when the system size $L$ increases. The data were fitted by

$$\langle e\rangle = e_0 + e_1 L^{-3/2} + e_2 L^{-2} + e_3 L^{-5/2}, \tag{29}$$

where the exponents were fixed as $-3/2=-y_{t1}$, $-2=y_{t2}-2$, and $-5/2=-y_{t1}-1$. After discarding the data for small system sizes $L\leqslant 12$, the fit yields $e_0=1.329\,377(4)$, $e_1=1.53(2)$, $e_2=-11.0(2)$, and $e_3=12.2(4)$, where we quote error margins of two standard deviations. The constants $e_1$ and $e_2$ have opposite signs. Similarly, we fitted the $C$ data by

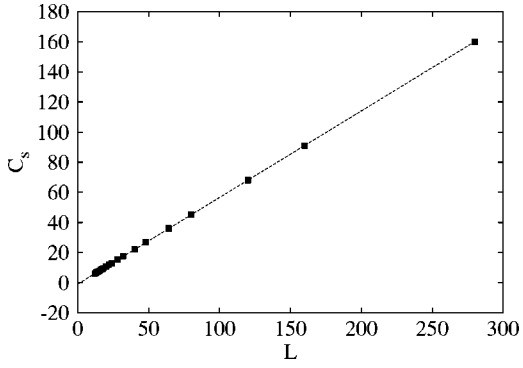


FIG. 15. Structure factor of the specific heat $C_s$ of the constrained dilute $q=4$ Potts model at the "fixed" point vs $L^{2y_{t1}-2}=L$. The approximate linearity suggests that the leading exponent for $C_s$ is still $y_{t1}=3/2$.

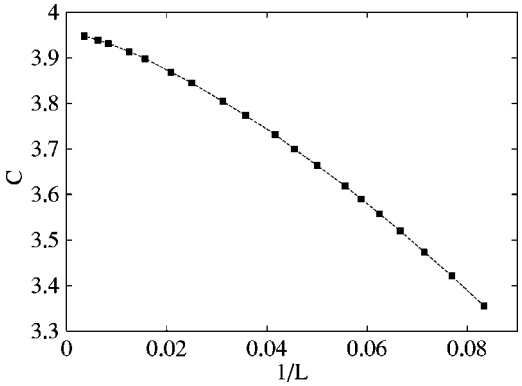


FIG. 16. Specific heat $C$ of the constrained dilute $q=4$ Potts model at the fixed point vs $L^{2-2y_{t1}}=1/L$. The significant curvature suggests that the approximation for the data of $C$ by the term with $c_1$ in Eq. (30) is insufficient.

$$C = c_0 + c_1 L^{-1} + c_2 L^{-3/2} \tag{30}$$

and obtain $c_0=3.960(4)$, $c_1=-2.1(4)$, and $c_2=-23(1)$. The amplitude $c_1$ is relatively small in comparison with $c_2$, which explains the strong nonlinearity in Fig. 16.

## V. DISCUSSION

The geometric cluster method serves well for a detailed investigation of the finite-size scaling behavior of constrained tricritical systems. For the $q=4$ Potts model with vacancies and the other systems, the constrained data can be explained by the second and first cases of the Fisher renormalization described in Sec. III, respectively. For clarity, a comparison of the unconstrained and constrained tricritical scaling behavior of several quantities is listed in Table II. These include the energy density $\langle e\rangle$, the specific heat $C$, the structure factor $C_s$, and the magnetic susceptibility $\chi$. These data illustrate that the scaling behavior of conventional energylike quantities is significantly modified under the constraint, while that of magnetic quantities and structure factors

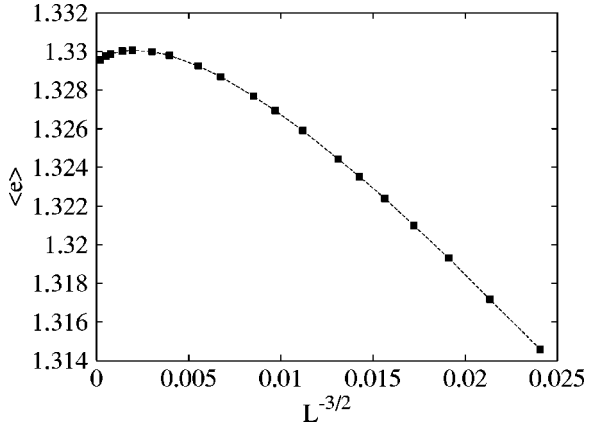


FIG. 17. Energy density $\langle e\rangle$ of the constrained dilute $q=4$ Potts model at tricriticality vs $L^{-y_{t1}}=L^{-3/2}$. The significant curvature suggests that the approximation for the data of $\langle e\rangle$ by the term with $e_1$ in Eq. (29) is insufficient.

TABLE II. Leading finite-size scaling behavior of $\langle e \rangle$, $C$, and $C_s$ of unconstrained (un) and constrained (co) tricritical systems, including dilute $q=1$, 3, and 4 state Potts models, the Blume-Capel (BC) model, and Baxter's hard-square (HS) model.

| Model | $q=1$ | BC | HS | $q=3$ | $q=4$ |
|---|---|---|---|---|---|
| $\langle e \rangle^{\mathrm{un}}$ | $L^{-1}$ | $L^{-1/5}$ | $L^{-1/5}$ | $L^{-2/7}$ | $L^{-1/2}$ |
| $\langle e \rangle^{\mathrm{co}}$ | $L^{-1}$ | $L^{-6/5}$ | $L^{-6/5}$ | $L^{-9/7}$ | $L^{-3/2}$ |
| $C^{\mathrm{un}}$ | $L^{7/4}$ | $L^{6/5}$ | $L^{6/5}$ | $L^{10/7}$ | $L$ |
| $C^{\mathrm{co}}$ | $\ln L$ | $L^{-2/5}$ | $L^{-2/5}$ | $L^{-6/7}$ | $L^{-1}$ |
| $C_s^{\mathrm{un}}$ | $L^{7/4}$ | $L^{6/5}$ | $L^{6/5}$ | $L^{10/7}$ | $L$ |
| $C_s^{\mathrm{co}}$ | $L^{7/4}$ | $L^{6/5}$ | $L^{6/5}$ | $L^{10/7}$ | $L$ |
| $\chi^{\mathrm{un}}$ | $L^{91/48}$ | $L^{77/10}$ | $L^{77/40}$ | $L^{38/21}$ | $L^{7/4}$ |
| $\chi^{\mathrm{co}}$ | $L^{91/48}$ | $L^{77/10}$ | $L^{77/40}$ | $L^{38/21}$ | $L^{7/4}$ |

remains unchanged. Generally speaking, the agreement between the numerical results and the theory is *quantitatively* satisfactory.

During the derivations of the scaling formulas in Sec. III, the Fisher renormalization mechanism makes essential use of the universal renormalization exponents in the unconstrained free energy density as described by Eq. (14). This simply means that the present annealed type of constraint does not modify the universality class, and thus the critical exponents in the constrained and unconstrained systems are directly related. We further demonstrate this point by investigating the scaling behavior of the structure factors $C_s$ and $P_s$, which remains unchanged under the constraint. Therefore, on the basis of the summary in the above paragraph, we conclude that the Fisher renormalization mechanism straightforwardly and completely describes the essential physics of the constrained scaling behavior. It then seems that there is no apparent need to apply other theories. Nevertheless, in this context, we mention Imry's theory [11,12,36] for constrained critical phenomena, which is more general and includes the Fisher renormalization mechanism [6] as a special case. This theory has been applied to the Baker-Essam model [35], a compressible Ising model, where a "special" tricritical point was reported. Such a point, where no renormalization of critical exponents occurs even for systems with $\alpha > 0$, has not been observed in the present investigation. For the experimental data [2] at the λ transition in the $^3$He-$^4$He mixtures, both the Fisher approach and the RG calculations of Imry and co-workers [13] can be employed. This has been further confirmed [14] by the Monte Carlo simulations of the tricritical Blume-Capel model in three dimensions. Although the RG calculations [13,36] can be regarded to correspond with the second case of the Fisher renormalization mechanism, as described in Sec. III, the connection of these two theories is not always obvious. Thus, it seems justified to ask the following questions: (1) In addition to the Baker-Essam model [35], can one further test the theoretical predictions in Refs. [11] and [12] in other systems? In particular, can one observe the aforementioned "special" tricritical point? (2) How are the RG calculations [13] related to the Fisher renormalization mechanism? (3) How can the effect of the subleading thermal field be included in the RG calculations [13]?

Although the mean-field theory is "unrealistic" in general, it can yield an intuitive physical picture of a phase transition. Moreover, for a sufficiently high spatial dimensionality, the mean-field theory can correctly predict universal parameters. Therefore, we investigated [14] the influence of the constraint on the mean-field version of the Blume-Capel model. Just as in finite spatial dimensions, the mean-field BC model has a line of second- and first-order transitions and a tricritical point. However, under the constraint, it can be shown that the whole transition line reduces to mean-field *critical* Ising like.

Finally, we remark that, in our application of the Fisher renormalization mechanism, *only* the leading terms are kept, as mentioned in Sec. III. It is obvious that including subleading terms leads to additional finite-size corrections besides those arising from the irrelevant scaling fields. In many cases [8–10,37,38], these additional terms can be important and thus should be taken into account properly. In fact, it was reported [37,38] that, in several *critical* systems, the leading terms of the constrained specific heat $C$ are so small that the finite-size scaling behavior of $C$ is mainly described by the subleading terms. Even for the percolation model in which $C$ is zero, a correction-to-scaling of an exponent $-0.503(4)$ exists [38] in two dimensions when the total number of occupied bonds and sites is fixed at criticality. In the language of finite-size scaling, the exponents for the subleading terms can be described [38] by $-n|2y_{t1}-d|$, where $n=1,2,\ldots$ is an integer. For the tricritical Potts systems in the present paper, these exponents are $-n7/4$ for $q=1$, $-n8/5$ for $q=2$, $-n10/7$ for $q=3$, and $-n$ for $q=4$. As a result, in comparison with the corrections due to the irrelevant scaling fields, the contributions from the subleading terms are insignificant and were frequently neglected in the present finite-size analyses.

## ACKNOWLEDGMENTS

We acknowledge valuable communications with Professor M.E. Fisher, Professor Y. Imry, and Professor J.M.J. van Leeuwen. This research is supported by the Dutch FOM foundation ("Stichting voor Fundamenteel Onderzoek der Materie") which is financially supported by the NWO ("Nederlandse Organisatie voor Wetenschappelijk Onderzoek").

[1] I. D. Lawrie and S. Sarbach, in *Phase Transitions and Critical Phenomena*, edited by C. Domb and J. L. Lebowitz (Academic Press, London, 1984), Vol. 9, p. 1.

[2] Y. Achiam and Y. Imry, J. Phys. C **10**, 39 (1977).

[3] R. B. Stinchcombe, in *Phase Transitions and Critical Phenomena*, edited by C. Domb and J. L. Lebowitz (Academic Press, London, 1984), Vol. 7, p. 152, and references therein.

[4] I. Syozi, Prog. Theor. Phys. **34**, 189 (1965); I. Syozi and S.

Miyazima, *ibid.* **36**, 1083 (1966).
[5] J. W. Essam and H. Garelick, Proc. Phys. Soc. London **92**, 136 (1967).
[6] M. E. Fisher, Phys. Rev. **176**, 257 (1968).
[7] Y. N. Skryabin and A. V. Shchanov, Phys. Lett. A **234**, 147 (1997).
[8] M. Krech, e-print cond-mat/9903288.
[9] I. M. Mryglod and R. Folk, Physica A **294**, 351 (2000).
[10] I. M. Mryglod, I. P. Omelyan, and R. Folk, Phys. Rev. Lett. **86**, 3156 (2001).
[11] L. Gunther, D. J. Bergman, and Y. Imry, Phys. Rev. Lett. **27**, 558 (1971); Y. Imry, O. Entin-Wohlman, and D. J. Bergman, J. Phys. C **6**, 2846 (1973).
[12] O. Entin-Wohlman, D. J. Bergman, and Y. Imry, J. Phys. C **7**, 496 (1974).
[13] Y. Imry, Phys. Rev. Lett. **33**, 1304 (1974); J. Rudnick, D. J. Bergman, and Y. Imry, Phys. Lett. A **46**, 448 (1974); Y. Achiam and Y. Imry, Phys. Rev. B **12**, 2768 (1975).
[14] Y. Deng and H. W. J. Blöte, Phys. Rev. E **70**, 046111 (2004).
[15] M. Blume, Phys. Rev. **141**, 517 (1966).
[16] H. W. Capel, Physica A **32**, 966 (1966); Phys. Lett. **23**, 327 (1966).
[17] R. J. Baxter, J. Phys. A **13**, L61 (1980); J. Stat. Phys. **26**, 427 (1981).
[18] D. A. Huse, Phys. Rev. Lett. **49**, 1121 (1982); R. J. Baxter and P. A. Pearce, J. Phys. A **16**, 2239 (1983).
[19] See, e.g., F. Y. Wu, Rev. Mod. Phys. **54**, 235 (1982).
[20] B. Nienhuis, A. N. Berker, E. K. Riedel, and M. Schick, Phys. Rev. Lett. **43**, 737 (1979).
[21] B. Nienhuis, in *Phase Transitions and Critical Phenomena*, edited by C. Domb and J. L. Lebowitz (Academic Press, London, 1987), Vol. 11, p. 1, and references therein.
[22] J. L. Cardy, in *Phase Transitions and Critical Phenomena*, edited by C. Domb and J. L. Lebowitz (Academic Press, London, 1987), Vol. 11, p. 55, and references therein.
[23] D. Friedan, Z. Qiu, and S. Shenker, Phys. Rev. Lett. **52**, 1575 (1984).
[24] X. F. Qian, Y. Deng, and H. W. J. Blöte (unpublished).
[25] P. D. Beale, Phys. Rev. B **33**, 1717 (1986).
[26] B. Nienhuis, J. Phys. A **15**, 199 (1982).
[27] See, e.g., D. Stauffer and A. Aharony, *Introduction to Percolation Theory* (Taylor & Francis, Philadelphia, 1994).
[28] R. H. Swendsen and J. S. Wang, Phys. Rev. Lett. **58**, 86 (1987).
[29] U. Wolff, Phys. Rev. Lett. **62**, 361 (1989).
[30] K. Kawasaki, in *Phase Transitions and Critical Phenomena*, edited by C. Domb and M. S. Green (Academic Press, New York, 1972), Vol. 2, p. 443.
[31] J. R. Heringa and H. W. J. Blöte, Physica A **232**, 369 (1996).
[32] H. W. J. Blöte, E. Luijten, and J. R. Heringa, J. Phys. A **28**, 6289 (1995).
[33] J. R. Heringa and H. W. J. Blöte, Phys. Rev. E **57**, 4976 (1998).
[34] K. Binder, Z. Phys. B: Condens. Matter **43**, 119 (1981).
[35] G. A. Baker and J. W. Essam, Phys. Rev. Lett. **24**, 447 (1970).
[36] Y. Imry (private communications).
[37] Y. Deng, *Conformal Symmetries and Constrained Critical Phenomena* (Delft University Press, Delft, 2004).
[38] Y. Deng and H. W. J. Blöte (unpublished).